Int. J. Adv. Eng. Pure Sci. 2022, 34(2): 288-304
DOI: 10.7240/jeps.1032186

RESEARCH ARTICLE / ARAŞTIRMA MAKALESİ

Computational Examination of Unsteady Cavitating Flow Characteristics on a 2D NACA66 Profile by Utilizing OpenFOAM®

Kararsız Kavitasyonlu Akış Karakteristiklerinin 2 Boyutlu Bir NACA66 Profili Üzerinde OpenFOAM® Kullanılarak Sayısal Olarak İncelenmesi

Samir Arda OĞUR[1], Emre ALPMAN[1]

[1] *Mechanical Engineering Department Marmara University, 34722, Istanbul, Turkey*

Abstract
The complexity of the flow mechanism is one of the crucial problems in cavitation. In this present study, detailed computational examinations of cavitating flow around a NACA66 hydrofoil were performed by using OpenFOAM® software. Dynamic and unsteady behaviours of cavitating flow were solved utilizing the *k-ε* and *k-ω SST* turbulence models. Schnerr-Sauer cavitation model was used for the calculations. Firstly, simulations were carried out by applying the same cavitation model (Schnerr Sauer) with the *k-ε* and *k-ω SST* model. The results were evaluated by examining the studies in the literature in terms of water volume fractions. After that with *k-ω SST*, numerical simulations were performed for 6° and 8° angle of attack with different cavitation numbers and the outlet pressure conditions, the cases are called "Case 1" and "Case 2" respectively. The results were compared with the studies performed by Leroux et. al. Oscillation cycles and flow characteristics were obtained successfully in both cases. The mechanism called the re-entrant jet was shown to be primarily responsible for cavitation break-off in two cases. This mechanism consists of two steps: 1) an interplay between the re-entrant flow and the cavity contact surface in the occlusion region, resulting in recurrent secondary cloud shedding until the primary cloud detachment, and 2) a shock wave triggered by the primary cloud collapsing, which affects the development of the remnant cavity.

The main contribution of this study is to demonstrate the superiority of the *k-ω SST* model over the other two-equation the *k-ε* model and examine the impact of using the *k-ω SST* turbulence model with the Schnerr-Sauer cavitation model on predicting flow characteristics such as cavitation dynamics, pressure distribution and cavity form. Reasonable accuracy has been observed for pressure fluctuations and cavitation dynamics.
Keywords: cavitation, cavitation break-off, *k-ω SST* model, NACA66 hydrofoil, OpenFOAM®

Öz
Akış mekanizmasının karmaşıklığı, kavitasyondaki en önemli problemlerden biridir. Bu çalışmada, OpenFOAM® yazılımı kullanılarak bir NACA66 hidrofili etrafındaki kavitasyonlu akışın ayrıntılı sayısal incelemeleri yapılmıştır. Kavitasyonlu akışın dinamik ve kararsız davranışları *k-ε* ve *k-ω SST* türbülans modelleri kullanılarak çözülmüştür. Hesaplamalar için Schnerr-Sauer kavitasyon modeli kullanılmıştır. İlk olarak simulasyonlar aynı kavitasyon modeli (Schnerr Sauer) uygulanarak *k-ε* ve *k-ω SST* modeller ile gerçekleştirilmiştir. Daha sonra *k-ω SST* modeliyle sırasıyla "Durum 1" ve "Durum 2" olarak adlandırılan çıkış basıncı koşullarına paralel olarak farklı kavitasyon sayılarına sahip iki farklı 6° ve 8° hücum açısı için sayısal simülasyonlar yapılmıştır. Sonuçlar, Leroux çalışmasının deneysel ve sayısal sonuçlarıyla karşılaştırılmıştır. Leroux deneylerine kıyasla her iki durumda da salınım döngüleri ve akış özellikleri başarılı bir şekilde elde edildi. Yeniden giren jet olarak adlandırılan mekanizmanın, iki durumda da kavitasyon kopmasından birincil olarak sorumlu olduğu gösterildi. Bu mekanizma iki adımdan oluşur: 1) ana bulut ayrılmasına kadar tekrarlı ikincil bulut dökülmesiyle sonuçlanan, yeniden giriş akışı ile kavitasyon arayüzü arasındaki, kapanma bölgesindeki bir etkileşim ve 2) ana bulutun çökmesi tarafından tetiklenen kalan kavitasyonun gelişimini etkileyen bir şok dalgası şeklindedir.

Bu çalışmanın ana katkısı, *k-ω SST* modelinin diğer iki denklemli *k-ε* modeli üzerindeki üstünlüğünü göstermek ve Schnerr-Sauer kavitasyon modeli ile *k-ω SST* türbülans modelinin kullanılmasının kavitasyon dinamikleri, basınç dağılımı ve kavitasyon formu gibi akış özelliklerinin tahmin edilmesi üzerindeki etkisini incelemektir. Basınç dalgalanmaları ve kavitasyon dinamikleri için kabul edilebilir doğruluk gözlemlenmiştir.
Anahtar Kelimeler: kavitasyon, kavitasyon kopması, *k-ω* SST model, NACA66 hidrofil, OpenFOAM®

I. INTRODUCTION

Cavitation is a very essential physical phenomenon that can emerge in many fields in connection with hydraulic machinery. It is an already well-known fact that hydraulic machinery applications generally face many problems such as brutal vibration, material damage and loss, noise, performance breakdown due to cavitation. Cavitation can be described as the rapid creation and implosion of vapour bubbles inside a liquid flow. The cavitation phenomenon occurs mainly when the flow field's static pressure goes down below the fluid's vapour pressure.

Corresponding Author: Samir Arda OĞUR, Tel: +90 531 860 88 18, e-posta: ardaogur@marun.edu.tr
Submitted: 03.01.2022, **Revised:** 18.05.2022, **Accepted:** 18.05.2022

Unsteady cavitation causes unwanted effects such as noise and vibration, which can lead to cyclic pressures, material loss, and performance degradation. As a result, an appropriate computational model and precise numerical simulation of cavitating flows are critical for predicting cavitation dynamics. It is beneficial and important to analyse them on a basic geometry with general measurements and compare them to previous authoritative studies.

The formation of the cavity-shedding process and the unsteady cavitating flow mechanism have been extensively studied. The transition from sheet to cloud cavitation has frequently been linked to a re-entrant jet at the cavity's edge. The role of the re-entrant jet in the cavity break-off process has been widely investigated using experimental and numerical methods. In general sheet cavitation on the suction side of a pump's blades, exhibits a pronounced unsteady nature. When the angle attack is minimal or the velocity is low, it mostly affects the back portion of the cavity, however, when the circumstances are more unfavourable, the whole vaporized region becomes unsteady, with peeling off big bubble structures on a regular basis. This second form, known as cloud cavitation, causes pressure variations from the cavity downstream, significant strains, and sonic dispersion owing to the implosion of cavitation bubbles near the wall surface. All these impacts are typically detrimental to the efficient working of an engineering applicant. Thus, it is critical to distinguish the various unsteady conditions that may emerge, as well as to comprehend the underlying physical principles that cause such instability.

Many authors have investigated cloud cavitation experimentally in two basic designs, namely, Venturi type sections [1, 2, 3] and two-dimensional foil sections [4, 5, 6, 7, 8]. The origin of flow instability is a recurring focus in all these papers. Until recently, the majority of studies have pointed to a re-entrant jet that travels from downstream to upstream at the flow separation zone. When the re-entrant jet reaches the contact surface of the sheet cavitation, the cavity separates, and the downstream side is re-emitted by the main flow until it collapses. This phenomenon, first proposed by Furness and Hutton [1], has lately been verified by experiments using electrical impedance probes and double optical probes. [1, 9]. Lush and Skipp utilized high-speed photography to examine cavitation in a duct flow, and they noticed periodical cavitation shedding caused by the re-entrant jet. The dye injection technique was implemented on an investigation of cavitation in a plano-convex foil to have an observation of re-entrant jets [10, 11]. Gopalan and Katz used particle image velocimetry (PIV) and The main objective of the computations is to accurately simulate the unsteady behaviours of cavitating flows. Cavitation models and turbulence models are essential to obtain accurate results from cavitating flow simulations. In cavitating flow simulation, the high-speed photography to examine the flow characteristics at the closure region and the sheet cavitation. It was discovered that the re-entrant jet forms when the cavity tends to close in an intense counter-pressure zone. Callenaere et al. examined unsteady cavitation and plotted the flow patterns with different stages involving the re-entrant jet. They realized the significance of an opposing pressure gradient in the formation of a re-entrant jet and, as a result, recurrent vapour shedding. These studies demonstrated that the cavity's cyclic pattern is significantly connected to the evolution of the re-entrant jet. This process is strongly dependent on the thickness of the cavity-forming over a backwards-facing step: cloud cavitation develops so far that very small contact exists between the re-entrant jet and the cavitation sheet interface [12, 13]. Furthermore, vortex generation in the cavity triggers the reverse pressure gradient and the growth and thickness of the re-entrant jet, resulting in cloud separation [6, 13]. Several hypotheses have been offered to clarify the creation of reverse flow: it might be caused by the collapse of the preceding vapour cloud [10] or by a process related to cavity growth [1, 14].

Additional physical mechanisms were also identified to support the flow instability: the cavity break-off was attributed to the interaction of the re-entrant jet and contact surface instability in the cavity's rear section [15]. A combined experimental and computational technique was implemented to examine the sheet/cloud cavitation dynamics around a 2D NACA0015 hydrofoil. Studies showed that the shock mechanism is the origin of cloud cavitation formation at low values of $\sigma/2\alpha$. They also explained the effects of shock waves created by the collapse of huge bubble bunches in the perspective of experimental or computational examination of cavitating flow around a two-dimensional 2D hydrofoil section. [5, 16]. Pressure pulses and partial cavity instabilities have been captured in cavitating flows on a NACA66 (mod) hydrofoil. At 6° and 8° incidence angles, two separate periodical behaviour with two different frequencies (dynamics 1 and dynamics 2) were demonstrated computationally. The re-entrant jet was shown to be the main cause of cavity break-off in both cases. Dynamics 2 represents the typical cavity's growth on the hydrofoil length following the flow separation process and resulting cloud cavitation. For dynamics 1, more intricate flow characteristics were observed. In this case, the periodical behaviour was obtained at a lower Strouhal number (~0.07/0.09) than dynamics 2. (~0.3) [8, 17]. Readers are encouraged to see Figure 5 and Figure 7 in [17] for details.

homogeneous hypothesis has been extensively applied. The cavitating region is regarded as a separate fluid with fully mixed vapour and liquid in this idea [18]. Two types of models are frequently used in support of this hypothesis. Firstly, the state equation model is

shown in [19] and [20]. In the partial cavity closure region, previous experimental studies demonstrated that the baroclinic torque factor is the most important element in the vorticity generation. The baroclinic torque component, however, cannot be adequately described by the state equation model since density and pressure gradients are always parallel. Secondly, the transport equation model, which is based on Rayleigh–Plesset equations and involves an extra equation for the volume fraction of vapour (or liquid) that incorporates condensation and evaporation components [21]. Many comparable cavitation models were implemented based on the transport equation model. The RANS equations, comprising the equation of mixture momentum and volume fraction for multiphase flows, were solved using an artificial compressibility approach with a specific modified formulation [22]. Moreover, a new cavitation model was utilized to simulate the unsteady cavitation in the nozzle and over a NACA 0015 hydrofoil. The results demonstrated its ability to resolve cavitation effects such as the periodical behaviour of cloud cavitation, the re-entrant jet evolution and the localised pressure peaks owing to the collapse of the bubble cloud. [23]. The "Full cavitation model" based on the expressions of phase-change rate, derived from a simplified version of the Rayleigh-Plesset equation, is developed in [24]. Flow parameters (velocity, pressure and turbulence) and pressure properties (saturation pressure, densities, and surface tension) influence these rates [24].

The applied turbulence model was recently found to be crucial in effectively predicting the unsteady process. Using a Reynolds average Navier-Stokes's equations (RANS) method with a standard 2-equation model, such as *k-ε* or *k-ω*, generally results in unrealistic flow stabilizations [25, 26]. Modifications are frequently added to these turbulence models to achieve commendable results for unsteady cavitation characteristics. Wu et al. proposed to use a filter-based *k-ε* model, which was first created by Johansen et al. [27]. The grid size specifies the filter in this approach, which avoids undue dissipation in slight moves while having a negative impact on substantial flow characteristics. Coutier-Delgosha et al. demonstrated that to produce periodic cavitation behaviours, it is required to estimate the impact of compressibility on the turbulence flow structures in the multiphase environment. The turbulent viscosity of the liquid/vapour mixture is slightly reduced because of these processes [27, 28, 19]. The shear stress transport As stated in the equation, the vapour volume fraction α is used to calculate the fluid density ρ and dynamic viscosity μ (2)-(3). The equations of the continuity and momentum are represented using index notation as follows:

$$1 - a_v = a_l = \frac{V_1}{V} \tag{1}$$

$$\rho_m = a_v \rho_v + (1 - a_v)\rho_l \tag{2}$$

SST k-ω model is one of the most prominent turbulence models (the model pretends to be *k-ε* as it moves away from the wall boundary surface while it pretends to be *k-ω* near the wall boundary condition) which gives better results for the flow characteristics of unsteady cavitation. [29]. The Reynolds-averaged Navier-Stokes (RANS) approach, which uses nonlinear eddy viscosity models, has been proved to improve prediction accuracy. The typical RANS approach fails to accurately estimate the shed-off cavity owing to the overestimation of the turbulent dynamic viscosity. Zhang et al. developed a hybrid RANS/LES model that accurately simulated the complex cloud cavitation stage. As an alternative or substitute, some of the RANS approach's traditional limitations may be resolved by using large eddy simulation (LES) or detached eddy simulation (DES) approaches, such as its inability to account for significant flow separation. This type of model is supposed to produce better computations of large-scale turbulent eddies, which will lead to more accurate predictions of large-scale flow unsteadiness. [30, 31].

In this study, *k-ε* and k-*ω SST* model in RANS methods were used for the simulation procedure. Even for large pressure gradient flows, standard two-equation models miss the separation and anticipate attached flow. The advantage of the *k-ω SST* model is that being one of the most reliable two-equation models for separation prediction. Compared to other approaches, the RANS method can achieve commendable results in less time, while LES and DES require a lot of computational time and cost. Moreover, considering the ease of application in 3-dimensional complex geometries in the following study, the RANS method was decided to use.

II. MATERIALS AND METHODS

2.1. Numerical Model

The numerical model resolves the equations of Reynolds averaged Navier–Stokes's (RANS) method. The solver operates the turbulence model which is combined with a cavitation model. The solver's features and equations are detailed in the hereafter.

The homogeneous equilibrium two-phase mixture method is implemented for the flow in a two-phase environment. The fluid is uniform in the vapour/liquid mixture model; therefore, the velocity and pressure of the multiphase fluid components should be consistent.

$$\mu_m = a_v \mu_v + (1 - a_v)\mu_l \tag{3}$$

$$\frac{\partial \rho_m}{\partial t} + \frac{\partial}{\partial x_i}\left(\rho_m u_j\right) = 0 \tag{4}$$

$$\frac{\partial(\rho_m u_i)}{\partial t} + \frac{\partial\left(\rho_m u_i u_j\right)}{\partial x_i} = -\frac{\partial p}{\partial x_i} + \frac{\partial}{\partial x_j}\left[(\mu_m + \mu_t)\left(\frac{\partial u_i}{\partial x_j} + \frac{\partial u_j}{\partial x_i} - \frac{2}{3}\frac{\partial u_k}{\partial x_k}\delta_{ij}\right)\right] \tag{5}$$

where ρ represents the fluid density of mixture; α signifies the volume fraction for each phase; l, m, and v are the subindexes of the liquid, mixture, vapour phases; μ_m denotes the laminar viscosity of mixture; μ_t indicates the turbulence dynamic viscosity; and i, j, and k symbolize the subindexes of the cartesian coordinate system.

2.2. Turbulence Model

The *k-ω SST* (shear stress transport) turbulence model is used in this work. This model provides *k-ε* and *k-ω* models to be utilized in combination in the same model. Thanks to the blending function in the formulations, the model acts like a *k-ω* near the wall boundary, while it acts like a *k-ε* model as it moves away from the wall surface. This model was discovered to ensure appropriate simulation results of boundary layer detachment characteristics, which was verified for the estimation of cavitation characteristics around the NACA66 hydrofoil. [29]

2.3. Physical Model of Cavitation

The vapour volume fraction mass transfer equation is used to simulate the cavitation process. The Schnerr-Sauer cavitation model [23], offered in the **interPhaseChangeFoam** solver, was applied for the numerical process. The vapour volume fraction is identified in equation (1). In equation (6) the transport equation is described. Significantly,$\dot{m}^+$ and $\dot{m}^-$respectively indicate the process of evaporation and condensation during multi-phase flow. [31]

$$\frac{\partial(p_v a_v)}{\partial t} + \frac{\partial(p_v a_v u_i)}{\partial t} = \dot{m}^+ + \dot{m}^- \tag{6}$$

The source terms $\dot{m}^+$ and $\dot{m}^-$ are defined in the following way:

$$\dot{m}^+ = C_v \frac{\rho_v \rho_l}{\rho} a_v (1 - a_v) \frac{3}{R} \sqrt{\frac{2(p_v - p)}{3p_l}} \tag{7}$$

$$\dot{m}^- = C_c \frac{\rho_v \rho_l}{\rho} a_v (1 - a_v) \frac{3}{R} \sqrt{\frac{2(p - p_v)}{3p_l}} \tag{8}$$

where C_c and C_v are coefficients relating to condensation and vaporization processes, and the suggested values are 2 and 1, respectively [31].

The Schnerr-Sauer cavitation model needs bubble number (N) value, which in this study was set to $1.6\text{x}10^{13}$. The bubble radius (R) was then calculated with bubble number (N) and vapour volume fraction (α_V)as given in equations (9)-(10):

$$a_V = \frac{N\frac{4\pi}{3}R^3}{1+\frac{4\pi}{3}R^3} \tag{9}$$

$$R = \sqrt[3]{\frac{3a_v}{4\pi N(1-a_v)}} \tag{10}$$

2.4. Numerical Setup

For the numerical procedure, the notional free stream velocity $Vref$ was set 5.33 m/s, relating to a formulation of the Reynolds number, $Re = Vref\ x\ c/v = 0.8x10^6$, where v indicates the kinematic viscosity of water and c denotes the hydrofoil's chord length. The actual incidence angles were set to 6° and 8°.

The flow conditions, which include the velocity of inlet flow $Vref$, the pressure P_∞ in the out of the domain, the cavitation number $\sigma = (P_\infty - P_{vap})/(0.5\rho Vref^2)$, ($P_{vap}$ signifies the water's saturation pressure; 2300 Pa, $0.5\rho Vref^2$represents the dynamic pressure and ρ denotes the den
sity of water) was successfully set in according to the angle of attacks.

The experimental process in [8, 17] is examined to guide the computational approach for obtaining cavitating flow. To prevent flow vaporization and step input effect computation is started with a higher-pressure value than it is in the outlet. The outlet pressure is reduced according to the desired σ value after the cavitation get completely lost and steady state condition occurs. It can be considered with examining pressure contours and alpha water values around the hydrofoil. Following that, the operating(exit) value is held constant, the computation is completed until one or two oscillation cycle is observed [17].

2.5. Hydrofoil and Computational Domain

The numerical investigations were implemented on the NACA66 hydrofoil, devised by the National Advisory Committee for Aeronautics (NACA).

During the numerical procedure, the hydrofoil is set with attack angles α = 6° and 8°. The arrangements are considered as case 1 and case 2. The cases were decided according to the **procedure in** [17]. The hydrofoil's chord length (c) is 0.15m. The readers are encouraged to look at figure 1 for a detailed description of the NACA66 hydrofoil. It illustrates the view of the hydrofoil profile with the α = 6° incidence angle, whereas figure 2 demonstrates the computational domain.

The computations are performed in a 2D domain. As indicated in figure 2, the inlet is placed 3c upstream of the hydrofoil centre of mass and the outflow is placed 11c downstream of the hydrofoil centre of mass. The width of the domain box is 5c. The hydrofoil's chord (c) is 0.150 m, while the hydrofoil span is selected at 0.01 m to generate the 2D domain.

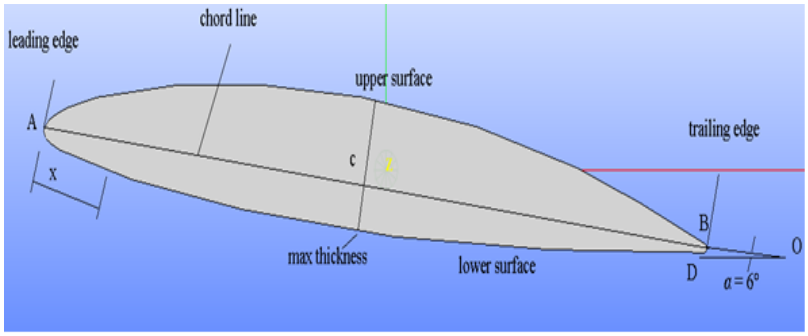

The relative maximum thickness of the hydrofoil is $\tau = 12\%$ at 45% chord length from the leading edge, and the relative maximum camber ratio is 2% at 50% chord length from the leading edge. The hydrofoil's chord length (c) is 0.15m.

Figure 1. Illustration of 2d NACA66(mod) hydrofoil

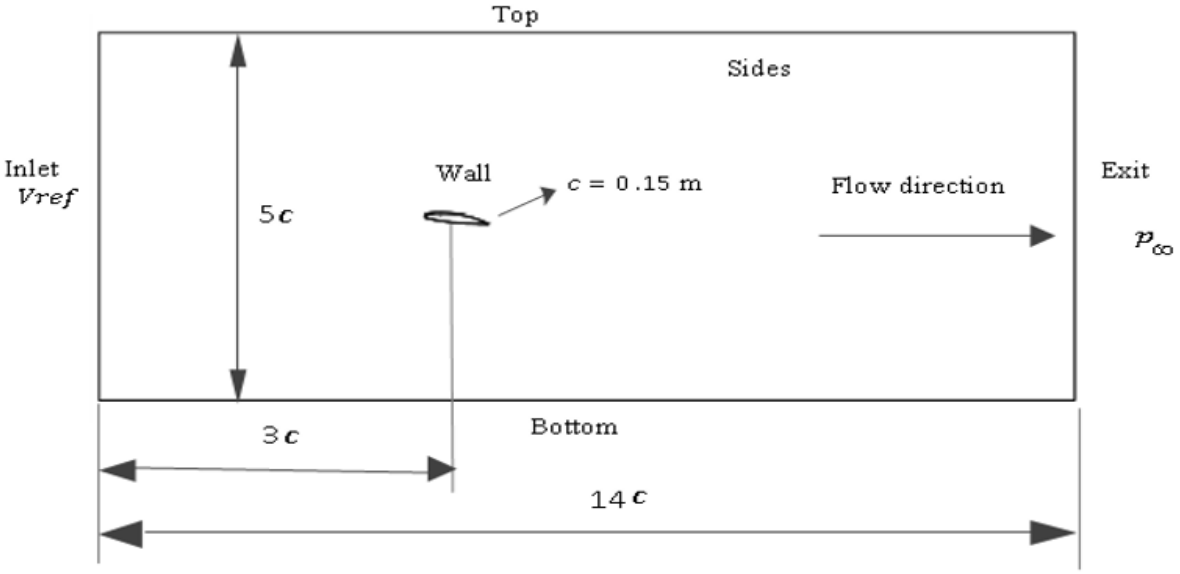

Figure 2. Computational domain

2.6. Boundary Conditions and Mesh

The boundary surfaces and the case conditions are defined in also figure 2 and table 1.

Figure 3 illustrates the meshes for the domain that were constructed with extra refinement near the hydrofoil's wall boundaries. Mesh generation was done utilizing SALOME (https://www.salome-platform.org/). SALOME is open-source software with fascinating capabilities for pre-processing and post-processing of simulation. The characteristics of CAD and meshing are combined to create a structured or unstructured grid for exporting in OpenFOAM®. The final points are about 490,000 with the type of prism cells.

The **kqRWallFunction** boundary condition was applied for turbulent kinetic energy (k), whereas the **nutUSpalldingWallFunction** boundary condition was applied for turbulence viscosity (μ_t) at wall boundary surfaces. The non-dimensional wall distance y^+ was calculated by the **postProcess** utility in OpenFOAM®. The maximum y^+ values vary between 30-50; These values were evaluated according to the values obtained from all time steps.

2.7. OpenFOAM® and Solver

Flow simulations involving cavitation are very challenging due to the phase alteration in the flow and the resulting sudden and high-density changes. Therefore, the solver that will be used for this study, must have the capacity to examine such multiphase flows. OpenFOAM® (https://www.openfoam.com/) offered some multiphase solvers in its library. Suitable solvers will be considered and used in the numerical procedure.

As an example, the **interPhaseChangeFoam** solver of the OpenFOAM® using the Volume of Fluid (VoF) method, has these properties and was previously used for cavitation analysis. It has been developed for the flow simulation of incompressible and immiscible fluids, involving phase change in an isothermal environment. [32]. Implicit Euler method was used for time derivatives and the unsteady solution of the equations. The Courant number (Co) was kept below 1.2 for the phase change flow visualization. The tolerances were set to 1.0e-8 for the pressure(p_rgh) and water volume fraction (alpha.water); 1.0e-6 for the velocity , k and omega computations. PIMPLE algorithm was arranged to operate five repetitions for

the convergence control.

Table 1. Boundary Conditions

Case Dynamics	Inlet	Exit	Top and bottom (far field)	Front and back. (sides)	Hydrofoil surface
Case 1(6° angle of attack σ =1.07)	Velocity $Vref$ = 5.33m/s	Pressure p_∞ = 17.499 kPa	empty	empty	wall
Case 2(8° angle of attack σ =1.25)	Velocity $Vref$ = 5.33m/s	Pressure p_∞ = 20.055 kPa	empty	empty	wall

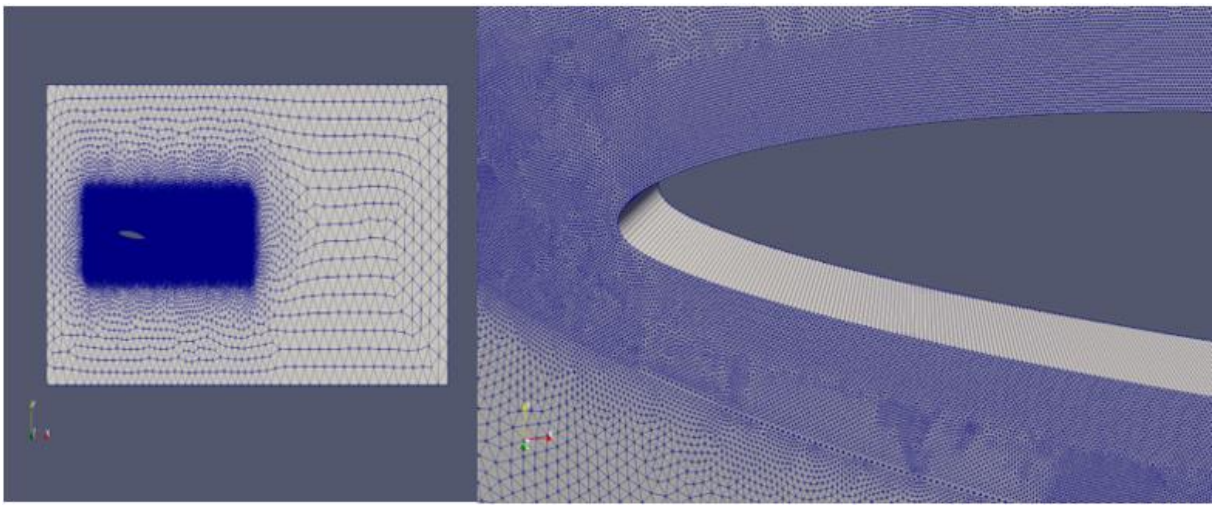

Figure 3. The view of unstructured mesh and mesh refinement around 2d hydrofoil

III. RESULTS AND DISCUSSION

In this study, computational investigations have been carried out to simulate the flow characteristics of cavitation around the 2D NACA 66 (MOD) profile. Initially, numerical simulations were performed with both *k-ε* and *k-ω SST* turbulence models by applying the same cavitation model (Schnerr Sauer). Solutions corresponding to the total real-time of 0.3 seconds are evaluated.

The water volume fractions obtained at different times are shown in figure 4. If this ratio is zero, it indicates that there is completely vapour in the region, and a ratio of one indicates that there is completely water. In the pictures, it is seen that the cavitation zone is getting wider and moving in the direction of the current. In previous experimental and numerical studies for this configuration [8, 17], the cavitation zone was separated from the hydrofoil surface during the growth phase and instantaneous cavitation decreases were observed on the hydrofoil surface. Readers are encouraged to look at figure 7 and 8 in [17] to examine the images that had 2been taken from different perspectives during the experiment and check the comparison of instantaneous void fractions for the cavitation dynamics. Although such characteristics are not observed in the results obtained with *k-ε*, it is thought that the reason for the difference seen with the experimental studies in the literature is that the boundary layer cannot be fully resolved, and the turbulence model used may be insufficient. As illustrated in figure 4, At the same time, the cyclic behaviours of cavitating flow characteristics could not be successfully simulated in the *k-ε* model. Flow separations, primary and secondary cloud ruptures were not observed in comparison to the solutions with the *k-ω SST* trial.

Numerical simulations were repeated with *k-ω SST* for both incidence angles (6° and 8°). The obtained results were compared with the numerical and experimental studies of Leroux et. al. [8, 17]. There were two unique cyclic behaviours specified as case 1 and case 2.

For case 2, the oscillation cycle was defined in accordance with the observations of the experiments by Leroux et. al. [17] as follows: cavity expansion with a

shiny contact up to roughly 60% of the chord length. Then the cavity is cut at about 10% of the chord by a re-entrant jet, moving upstream, which leads to the roll-up of the cloud. After the roll-up finishes, the cloud detachment occurs. Finally, the cloud collapses while the remnant cavity develops again. The numerical calculation accurately reproduces the fully unsteady process, as illustrated in figure 5. The volume fraction of water was demonstrated during the process. The red areas represent the vapour phase, and the blue areas represent the water phase. In Figures 1-4, blue regions were observed between the red regions. These blue regions clearly show the re-entrant jet formation and flow separations where the water phase divide between the two cavitated regions. Picture 2 in figure 5 shows us the cavity break-off, following pictures 3 and 4 demonstrate cloud detachment. Picture 5-8 represents the stage of the remnant cavity growth after cloud separation. The new red area growth from the hydrofoil's trailing edge to the mid chord can be seen while the other sizeable, red-zoned bubble clusters detach in pictures 5-8. Both the periodical behaviour and the maximum attached cavity length are in good agreement with [17]. The computational results demonstrate that the cloud separation is triggered by a re-entrant jet: when it reaches the cavity's forefront and destroys the contact surface of multiphase interaction, the cavity breaks off.

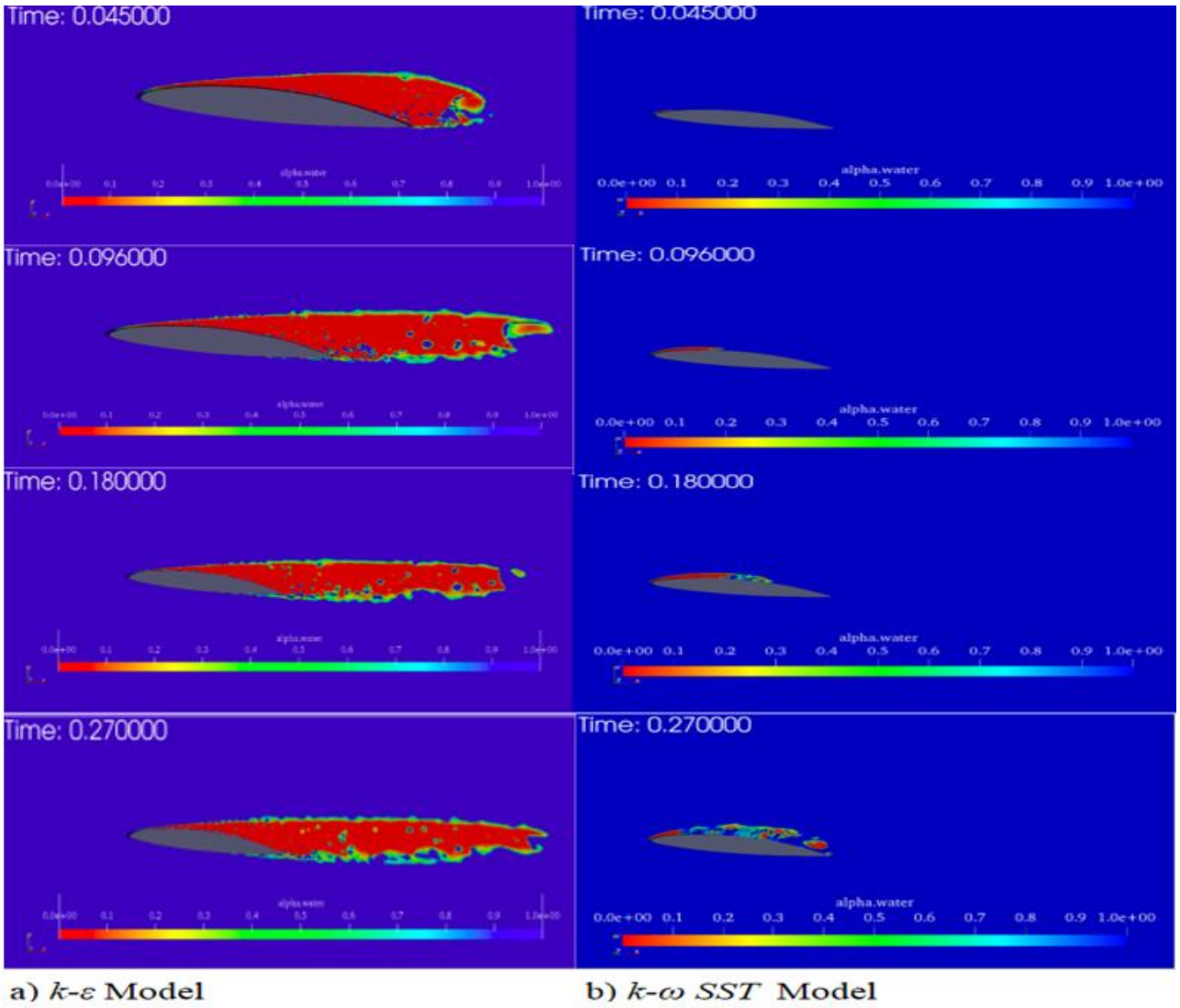

Figure 4. The comparison of the water volume fraction fields solutions for two different turbulence models.

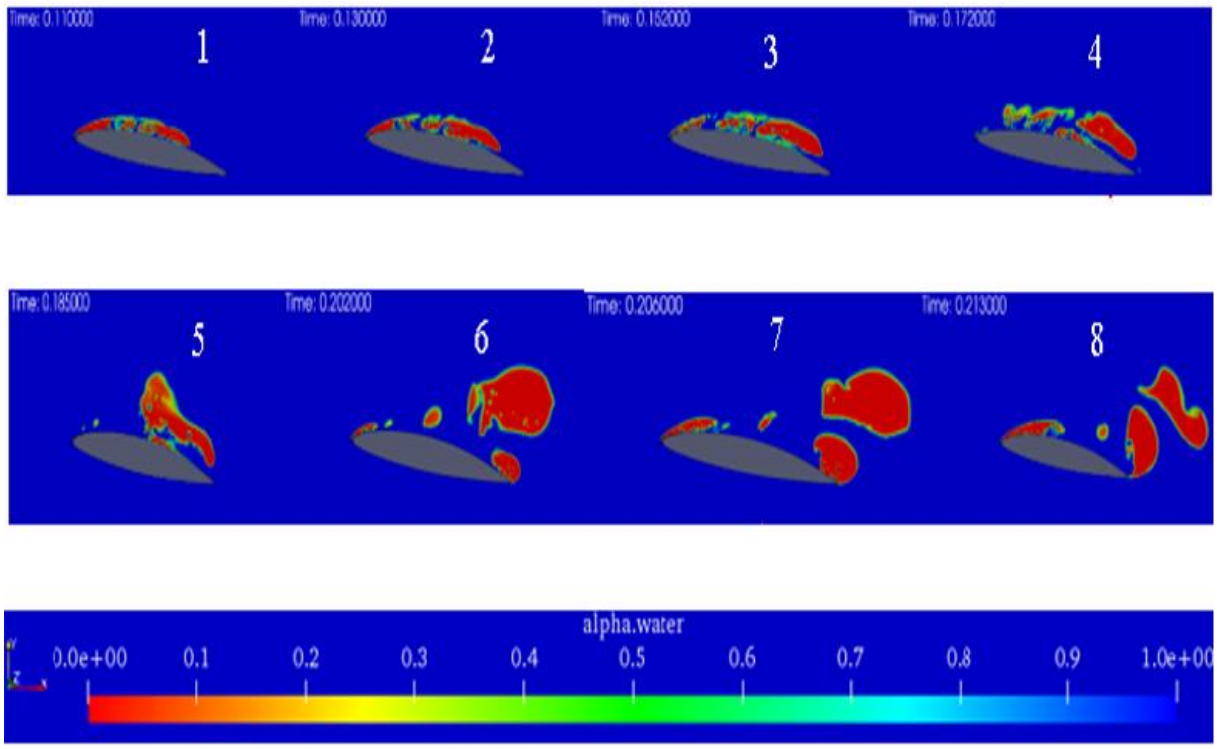

Figure 5. The illustration of primary and secondary cloud collapse in case 2(8° incidence angle, $Vref$ = 5.33 m/s, σ = 1.25

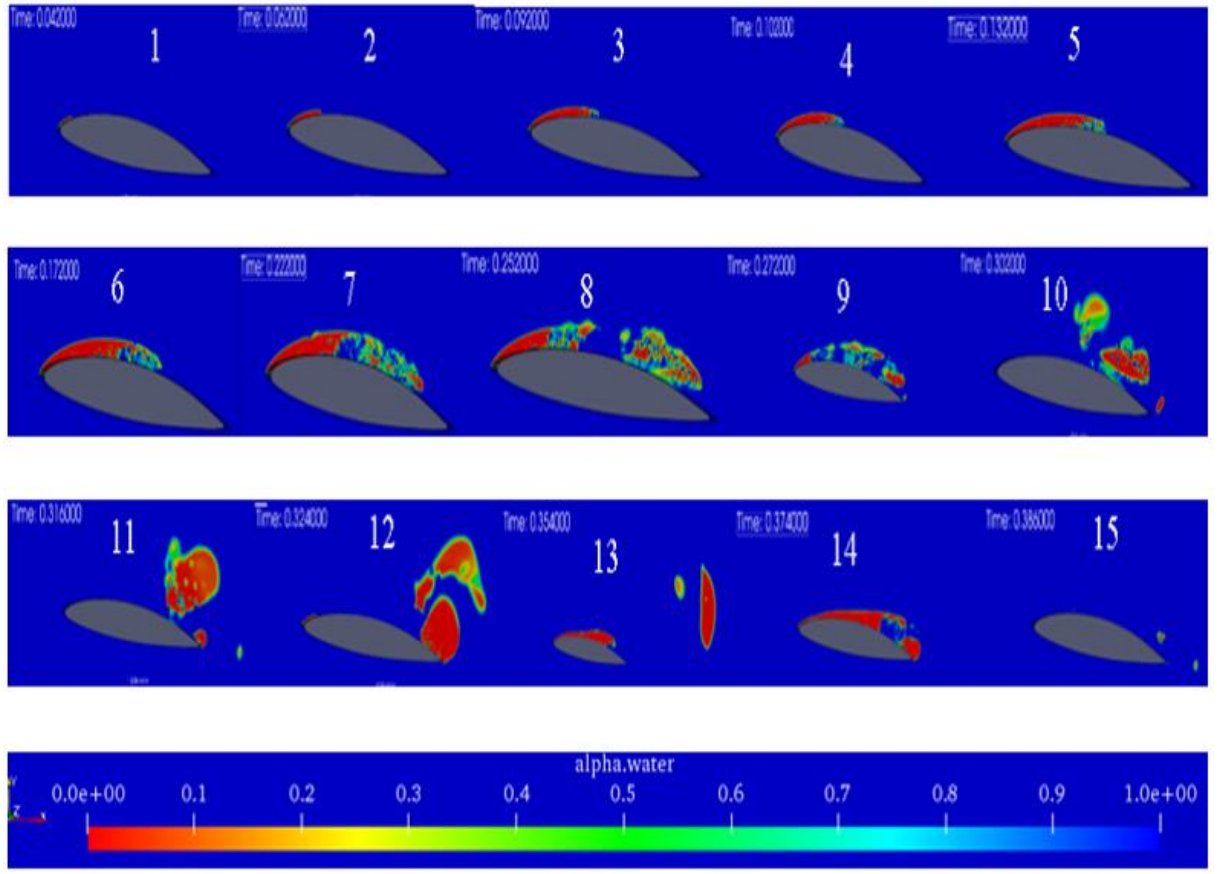

Figure 6. The unsteady periodical cycle of case 1(6° incidence angle, $Vref$ = 5.33 $m/s, \sigma$ = 1.07)

Cyclic vapour cloud shedding is still observable for case 1. The periodical behaviour of case 1 was also described in [17]. The cavity behaviour is more complex, as shown in figure 6. It can be explained by two steps: The cavity expands up to 60% of the chord, after which it is decelerated and is counterbalanced by the exuviating of vapour formations (secondary cloud) in the eddy. According to the comprehensive flow simulations, the peeling of the minor vapour clouds is assumed to be triggered by the collaboration of the re-entrant jet and the cavity junction in the cavity's rear half. The exuviation of a major vapour cluster (primary cloud) emerges following the exuviation of subsidiary clouds. The primary cloud rolls up and convects while the remnant cavity grows. After the cavity break-off, the second step takes place. Indeed, the expansion of the residual cavity comes to a halt practically simultaneously with the main cloud collapse, and the residual cavity virtually vanishes. The cavity subsequently begins to grow again, creating cavitation finger patterns that eventually merge to create cavitating patches and finally cavitation. The extra step before the next cavity grows causes a cycle delay.

Similar cavitating conditions were investigated numerically. Commendable results are obtained for case 1 in terms of the periodical behaviour and the maximum attached cavity length. Water volume fraction fields are given in figure 6 during the oscillation cycle. Colour zones between blue and red indicate that the volume fraction of water is between 0 and 1. The slow increase of the cavity length step is successfully illustrated (picture 1-6). Between picture 1-6 red zones which represents the cavitated vapour region gradually expands towards the mid-chord and reaches approximately 60% of the chord length. From this moment on, it is clearly illustrated in picture 7 that the red-coloured cavitated areas are separated by the blue-coloured water-phase areas. It means that the re-entrant jet, along with flow separations, caused the stage for secondary vapour collapse. The secondary vapour shedding (picture 8 and 9) transforms into the biggish red zones which represent largish vapour bulks in picture 10 and starts the stage of main cloud detachment (picture 11). They are also in the correct order. The following stage of primary cloud collapse is the regrowth of the red-coloured region from the trailing edge as the largish bubble clusters peel off. (pictures 12,13) Then finally the abrupt disappearance of the cavity once the vapour cloud collapses (pictures 14,15) are also accurately captured. It is seen that the cavitating red-coloured vapour region has completely left its place in the blue-coloured region on the hydrofoil surface.

Nevertheless, the simulation estimates a higher growth of the remaining cavity against the experimental studies by Leroux et. al. [8, 17]. Finally, even though the re-entrant jet could not be captured during the experiments, simulations show that it is still in charge of cavity cut-off from the contact surface and primary cloud separation Velocity profiles during the vapour cloud separations are illustrated in figure 7. Close to the hydrofoil wall, the opposite flow is observed travelling upstream until its head surpasses the cavitation sheet's border near the leading edge. Readers are encouraged to look at figures 7 and 9 in [17] to assess the results and similarities in the pictures.

Numerical simulations were completed successfully without any diverging problems. The maximum Courant number was set to 1.2 and accordingly, the analysis time step is 1.0 e-05. As explained in the previous sections, the necessary relaxation tolerances for the Gauss-Seidel algorithm were given in the solver settings. For robust convergence control, the PIMPLE algorithm was set to repeat with 5 outer correctors iteration during each time step of the analysis for pressure calculations. Limiter iteration number had also been arranged the value of 5 for the water volume fraction calculations. Residuals were plotted after the simulation is completed. As can be seen in figure 8, the number of iterations for "alpha.water" and "p_rgh" is 5 times larger than for "k" and "omega". In addition, it is also noticed that the tolerance values set are different.

In this study, a mesh refinement study was performed to investigate the effect of the mesh number on the hydrofoil region on the cavitating flow characteristics and flow conditions. In Case 1, mesh refinement was applied to an elliptical area, including the hydrofoil wall surface area. In the first case, the mesh contains approximately 317,000 thousand prism cells and is called "mesh". The second condition, together with the mesh refinement applied to an elliptical zone which consists of the wall surface of the hydrofoil, contains around 490,000 prism cells and is called "refined mesh". Finally, in the third condition, mesh refinement was made in the intense hydrofoil region, increasing the total number of prism cells to 980,000 and it was named "refined mesh2".

When a cross-section is taken from the wall surface of the hydrofoil after the first refinement, it is observed that the pressure values on the cross-section and the water volume ratio values for the two conditions match and show the compatibility up to the moment t=0.17. The comparison is illustrated in figure 9. After t=0.17, the "refined mesh" condition had estimated the pressure fluctuations more accurately than the first mesh. This can be decided by examining the alpha water fields. It was observed that the cavitating flow characteristics could not be observed for the first mesh condition after t=0.17 and the cavity extending up to the mid chord length did not transform into another cavitation dynamics until the end of the analysis. This is primarily due to the inadequacy of estimating the pressure values for the first mesh. However, the results obtained with the "refined mesh" were found to be sufficient when the cyclic behaviour of cavitating flow patterns was evaluated.

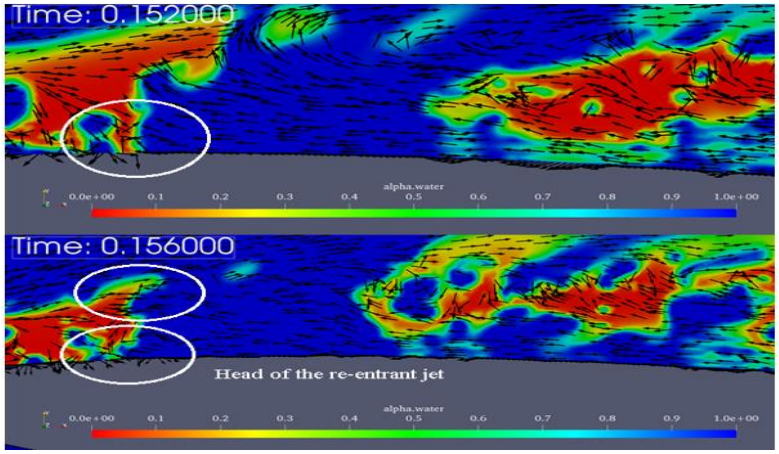

Figure 7. Flow separations and cavity break-off (case 2: 8° incidence angle, $Vref$ = 5.33 m/s, σ = 1.25)

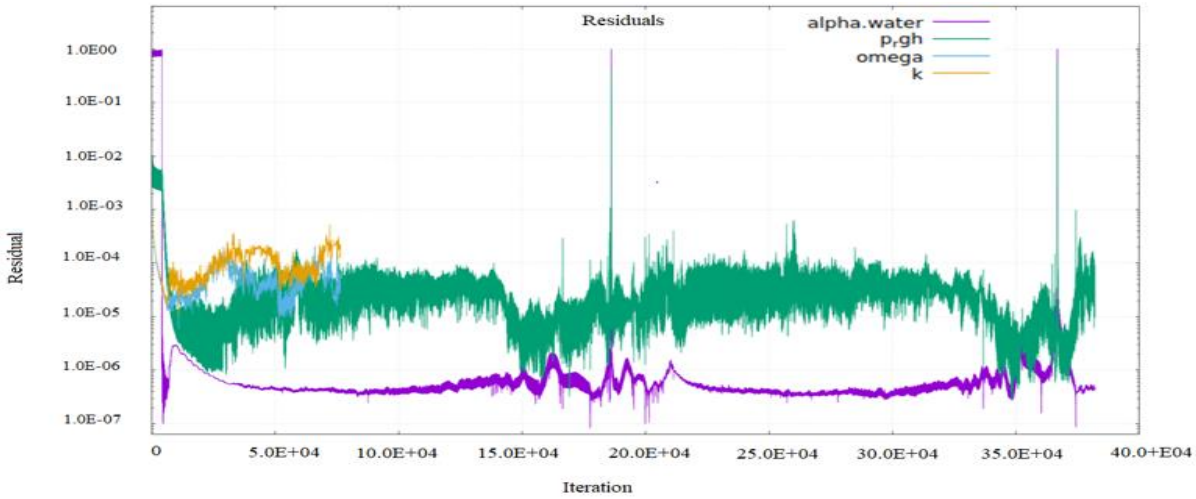

Figure 8. Residuals of the analysis

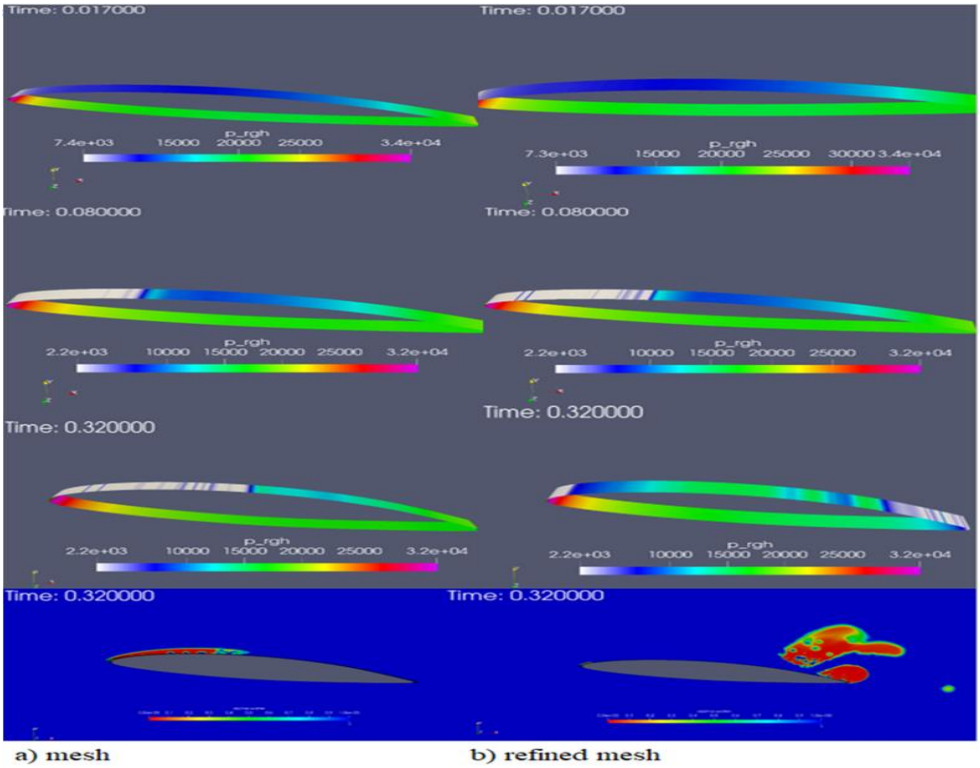

Figure 9. Pressure distribution and alpha water fields comparison for two different mesh

After the second refinement, the results were expected to be better than the previous one, but at the beginning of the simulation, noticeable changes and differences in the pressure values were detected. The fact that these values are so different compared to the previous predictions completely changes the cavitating flow behaviour. Looking at the graphs in figure 10, pressure fluctuations graphs are given for all 3 conditions. The yellow line in the graph represents the pressure values obtained with the initial mesh, and the green line represents the pressure values obtained with the refined mesh for the first time. The dark red line in the graph shows the pressure values obtained after the last refinement. The initial and final mesh conditions are called "mesh", "refined mesh" and "refined mesh2" in the legend bars, respectively. As can be seen from the graph, the cavitation process could not start correctly despite the mesh being refined for the second time. This can be understood by looking at the previous "mesh" and "refined mesh" values. It is thought that the reason for this uncertainty in the mesh refinement study may be due to the unstable, completely turbulent and chaotic problem of cavitation, as well as the pressure reduction method applied for simulations.

According to the investigations, cavitation disappears after a while after the start time of the simulation for the formation of cyclic cavitation characteristics. We can understand this by looking at the fact that the alpha water values between t=0.010-0.017 in the analysis are 1 and the interface Courant number values are 0. During the studies, cavitation disappears after t=0.01 in the "mesh" and "refined mesh" conditions. After monitoring the pressure values between 0.01-0.017 and making sure that they do not change and that cavitation does not start, the high-pressure value given at first is adjusted to the outlet pressure value calculated according to the required cavitation number and the simulation continues from where it left off. After a certain time from this moment, the cavitation proceeds from the leading edge in a healthy way. However, in the "refined mesh2" condition, the intense mesh applied to the hydrofoil surface region causes the cavitation to disappear for a short time at a value of approximately t=0.0161 between t= 0.016 - 0.017 and to start again in the timesteps after t=0.017. Since the pressure values could not reach the steady-state condition within a certain time interval, cavitation could not be formed properly. The cavitation process was failed to start, resulting in a complete change in cavitating flow patterns. As a result, it was decided to make all the evaluations in this article according to the results in the "refined mesh" condition containing approximately 490,000 prism cells.

The pressure distributions on the hydrofoil surface are the most important parameters for the correct observation of unsteady cavitating flow structures. Pressure values affect cavitation formation and therefore water volume fraction values. In figure 11 pressure distribution comparisons between numerical and computation studies are illustrated. The comparison has been investigated for σ=1.25 and α = 6° incidence angle. The experimental values were obtained from figure 10 in [8]. Readers are encouraged to look at figure 1b in [8] to check the pressure measurement locations for the experimental setup. As can be seen from the graph in figure 11, the reason for the initial pressure being overestimated is due to the high initial pressure given by the method applied. After a short time, the pressure value in the simulation came to values close to the results in the experiment. In this respect, commendable results were obtained between numerical computation and experiments. However, the pressure values were not only investigated quantitatively in this paper. The transition relations between the peak values of pressure fluctuations and the stages of cavitating flow dynamics were evaluated and compared qualitatively by examining the studies in the literature [17]. Experimental results for pressure fluctuations could not be used quantitatively in these comparisons. The reason why numerical value comparison could not be applied can be explained as follows. First, the criterion value used for pressure fluctuations in the study in the literature is different. Experimental and computational pressure data were compared according to the criteria called "wall pressure fluctuations" is defined $p' = p - p_{moy}$. Readers are encouraged to examine figure 12 in [17] to check how the p' values can vary. It is noticed that p' (Pa) can take negative values, so the criterion is different. Secondly, the differences in cycle periods can be shown as another reason.

Pressure fluctuations were also considered qualitatively for both cases. The pressure values are examined for the different locations (which are respectively 30%, 50%, 70%) on the chord length. The pressure values demonstrate the periodic behaviour of cavitation dynamics. Figure 12 shows the pressure values (on three different locations in terms of x/c) obtained from simulations until the beginning of the second cycle. Due to the complicated cavity behaviour, four sequences have been recognized for each period: the growth of the cavity (1), separation of primary cloud (2), the following cavity development (3), and sudden disappearance owing to cloud collapsing (4). According to the results in [17], the residual cavity shows a little rise at every x/c on the chord length, but the calculation anticipates a greater increase. Moreover, the start and end times of the sequences do not exactly match the numerical and experimental results by Leroux et. al. [8, 17]. This difference is due to the approach used for numerical simulation. Because to make calculations in a system where steady-state conditions have been reached and to eliminate input effects, the pressure was given at a value higher than the required one and the pressure was applied after the desired conditions were reached. In addition, the pressure reduction method after the first given pressure

will also affect the formation of the desired conditions and, accordingly, the start time of the cavitation cycle and stages. Giving the desired pressure too high and gradually decreasing it or giving less and then suddenly pulling to the desired value and continuing the simulation can completely delay the cavitation start time and all other sequences. Furthermore, the turbulence model used can also affect the time of the cycle steps. The k-ε *RNG* model had been used for calculations in [17], readers are encouraged to check the graphics of figures 12 and 14 in [17] to see the discrepancies between computational and experimental results. The important thing here is that the *SST k-ω* turbulence model was able to show the cavitation characteristics and oscillation cycle steps acceptably, as can be seen from the graphics in figure 12. After the pressure in the graphs is at its highest (t=0.385), the pressure values suddenly decrease while the cavitation suddenly disappears. To explain the relationship the pressure fields and water volume fraction values were examined in detail in the range of 3-4 sequences. It is illustrated in figures 13 and 14. It has been noticed that there is a mechanism that causes the pressure to peak between the progression of the remaining cavity and the sudden decrease in cavitation.

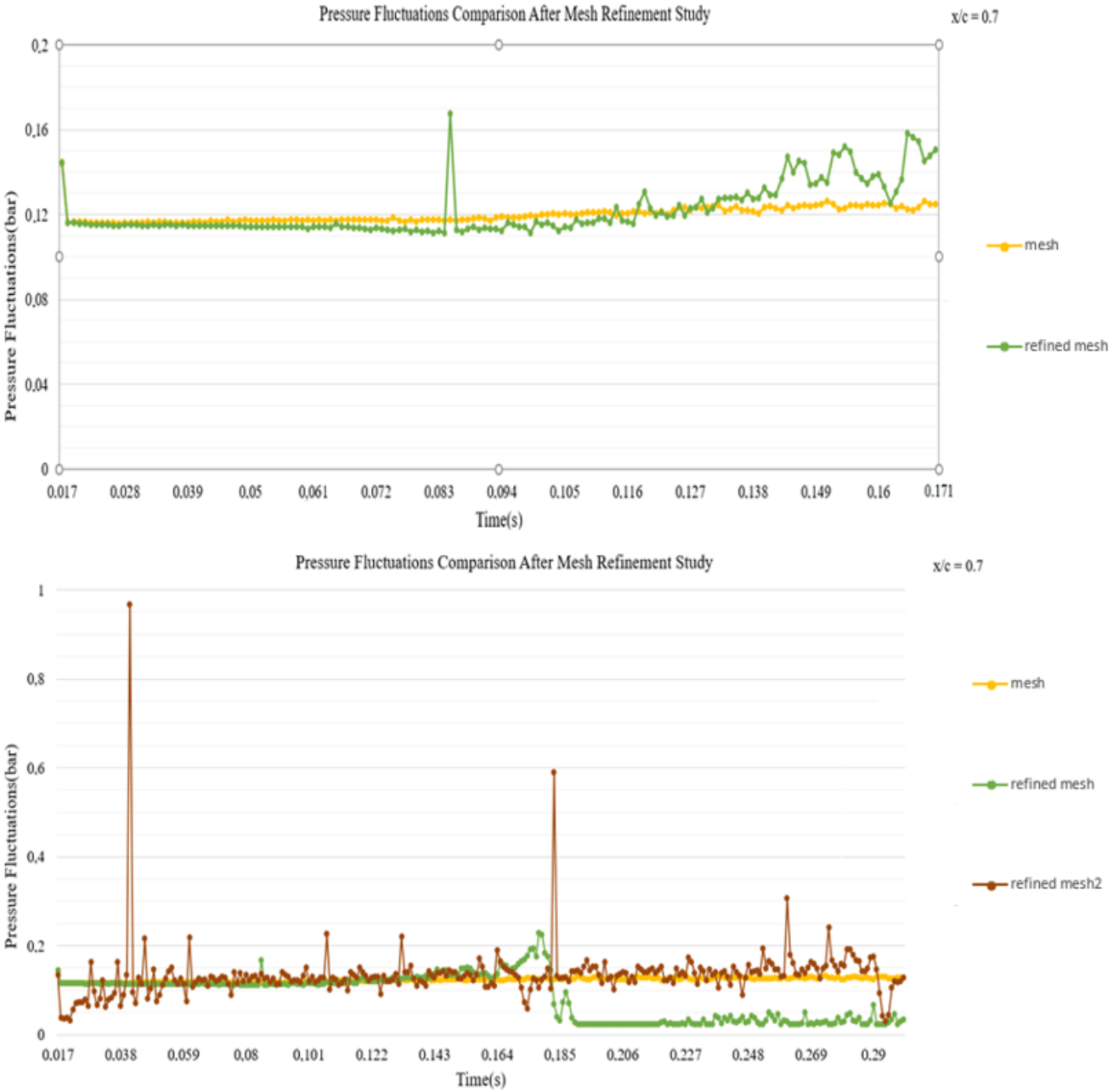

Figure 10. Pressure fluctuation comparison after the mesh refinement study

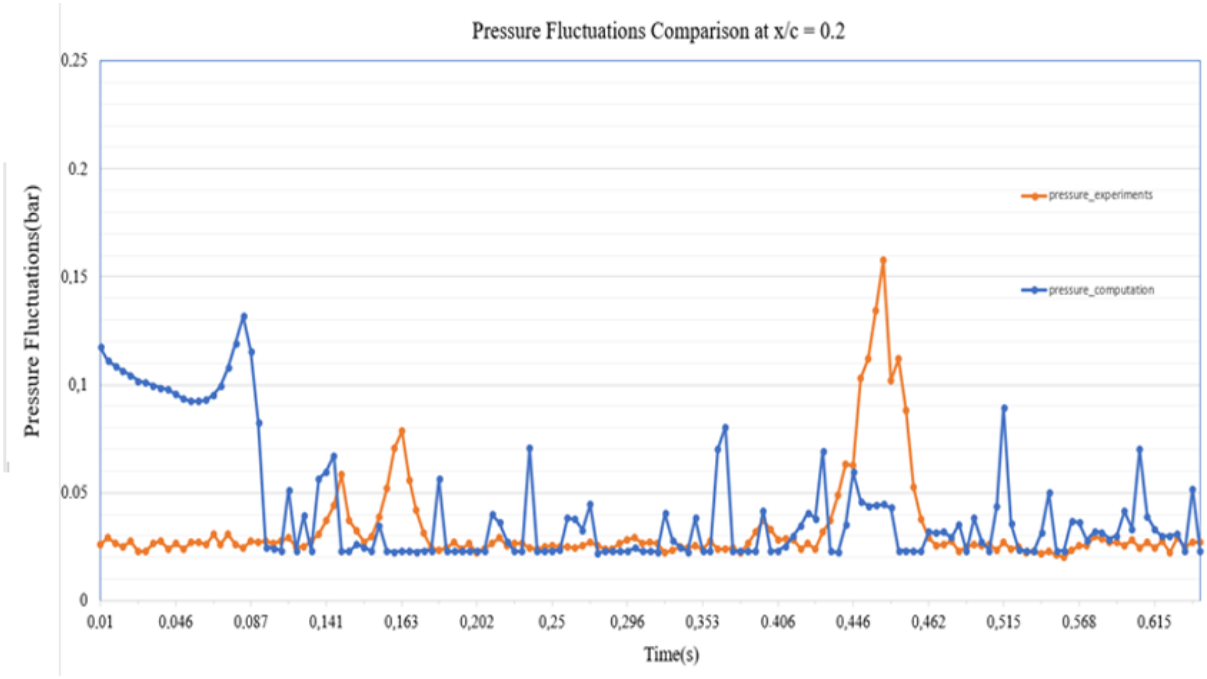

Figure 11. Pressure fluctuation values comparison, σ=1.25 and α = 6° incidence angle

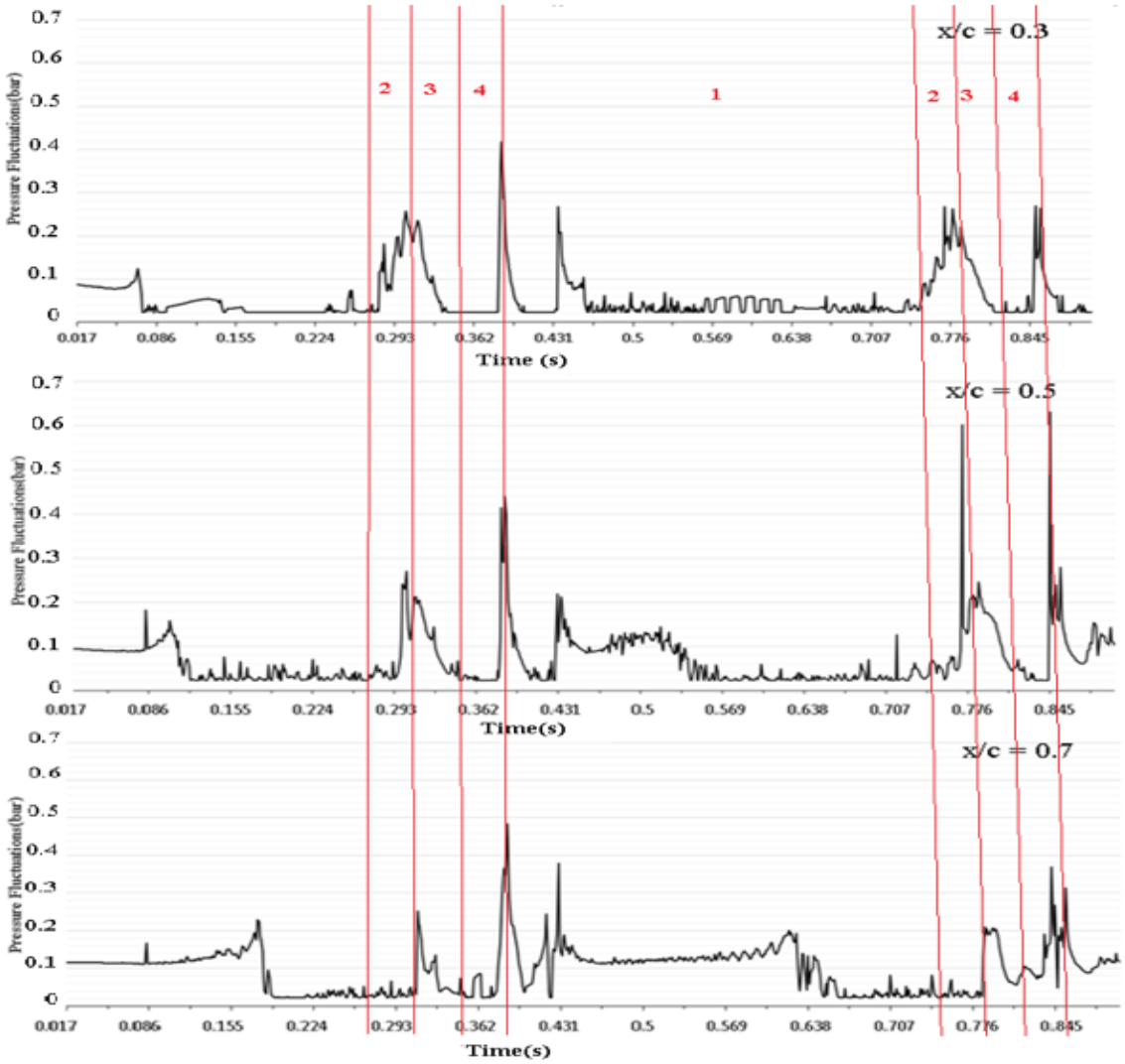

Figure 12. Pressure values overtime on the different locations of the hydrofoil's suction surface for case 1

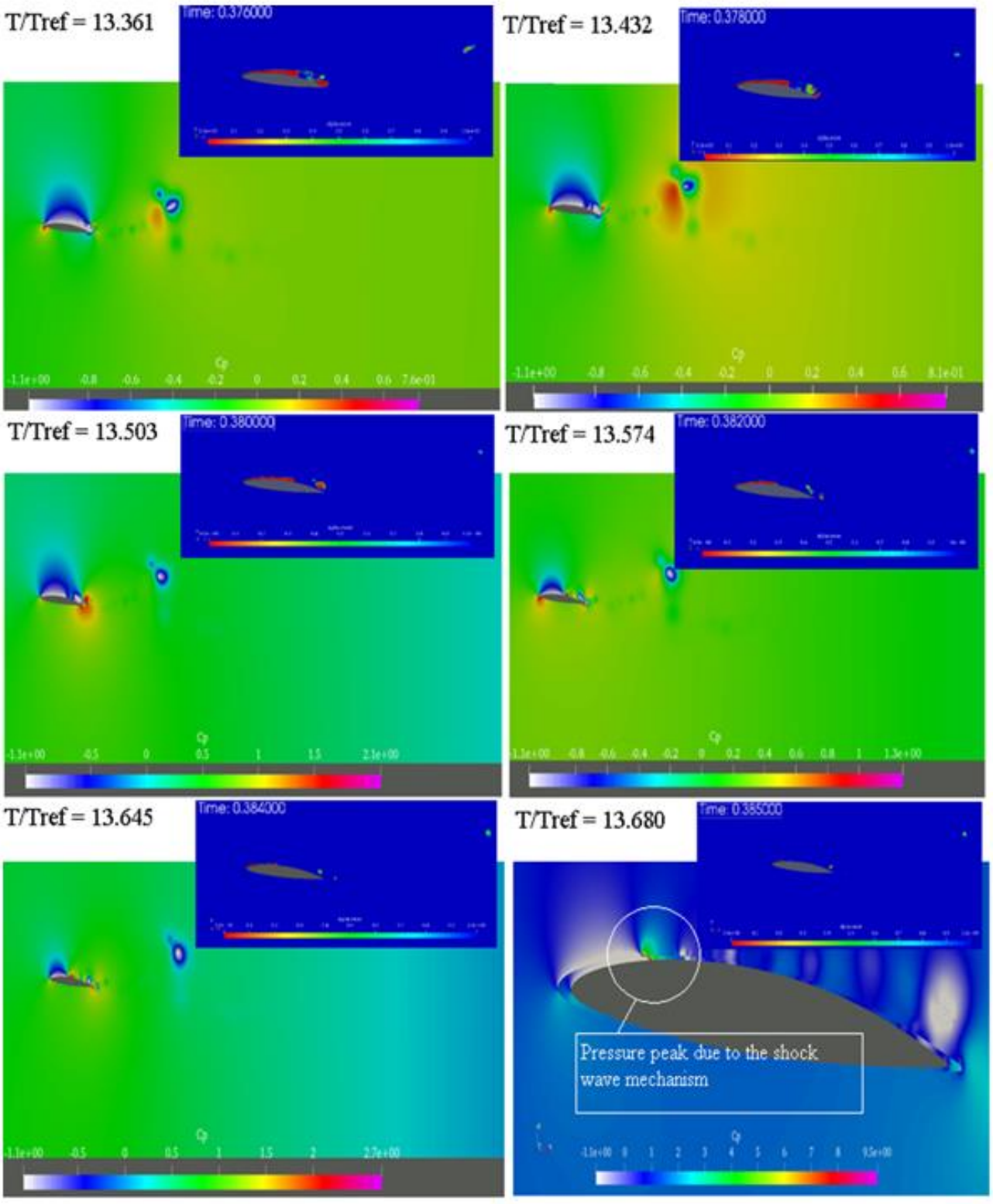

Figure 13. Pressure and alpha water distributions during the vapour cloud collapse and the abrupt disappearance of the cavity. Case 1(6° incidence angle, $Vref = 5.33\, m/s, \sigma = 1.07$)

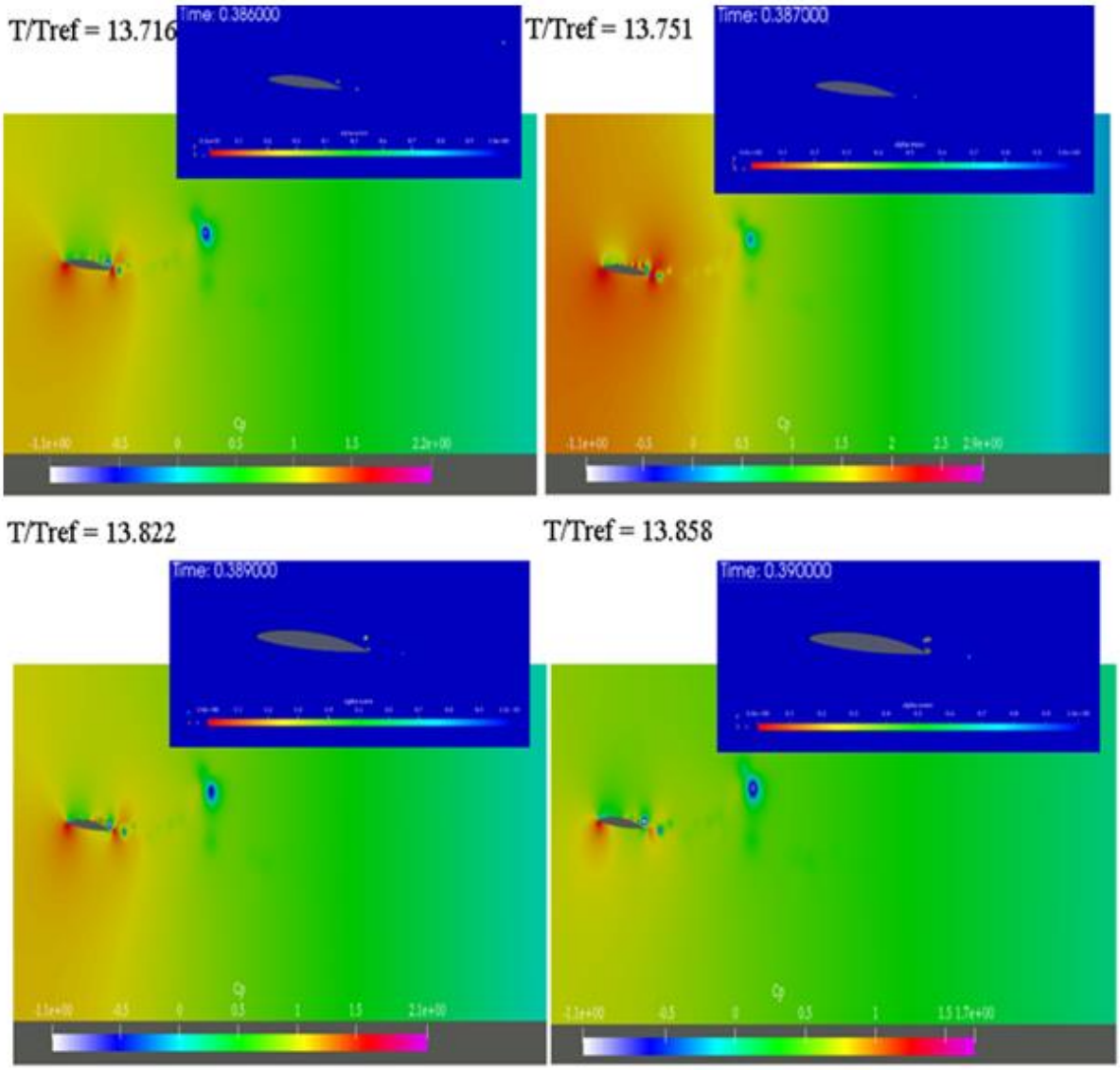

Figure 14. Pressure and alpha water distributions after the abrupt disappearance of the cavity. Case 1(6° incidence angle, $Vref = 5.33\ m/s,\ \sigma = 1.07$)

IV. CONCLUSIONS

In this paper, flow structures and the dynamics of unsteady cavitation have been numerically simulated. Firstly, the *k-ε* model and then the *SST k-ω* model were used for turbulence and their performance for cavitation prediction is compared. After it is concluded that the flow physics could be better captured with the *SST k-ω* model, the following calculations were carried out with this model in the 2D hydrofoil section arrangement. Cavitating vapour detachment for two individual dynamic cycles (case 1 and case 2) was obtained at respectively 6 and 8 degrees of attack. They are defined by two separate periodical behaviour. The process is more complicated for case 1. When the cavity expansion reached nearly 50%-60% of the chord, it was decelerated and alternated by the cloud shedding. The secondary clouds formed as a result of an interplay for both the re-entrant jet and the contact surface in the growing cavity's rear side. (as in case 2.) The cavity closure oscillated during secondary cloud shedding until a substantial disruption emerged, dividing the cavity into two separate components:1) a remnant cavity growing until approximately 20% of the hydrofoil chord length and 2) sizeable cavitating vapour phase (primary cloud) evolved downstream. The remaining cavity regrows until it completely disappears, as also observed in [17]. Although the re-entrant jet was not clearly illustrated by pressure fluctuations results, numerical simulations revealed that it played the leading role in flow separation and formation of primary cavitating cloud.

This is believed to be the result of the major cloud collapse closed to the trailing edge, causing a "shock wave" effect. The rapid decrement of the remnant cavity appears to be linked to the major cloud collapse, according to both experimental and numerical observations. The pressure evolutions on the hydrofoil's suction surface, as well as the consecutive

stages of the unsteady processes, were found to correspond well together with experiments and numerical computations. The numerical results were examined to express the differences in behaviour between the two cases. The collapsing process was studied to seek probable cavity dynamic feedback from the vapour implosion. It was observed that a pressure wave spreads with a high level of velocity when the cavitation suddenly disappears. It travelled from the collapsing point to the direction of the domain outlet. This phenomenon was observed in both cases.

In conclusion, it has been shown that the *k-ω SST* turbulence model can be used to determine cavitating flow characteristics on a 2D hydrofoil using OpenFOAM®. The *k-ω SST* model has proven superiority over the other two-equation *k-ε* model in simulating flow separations, cavity dynamics and re-entrant jet formation. The numerical procedure will be utilized in the following work to simulate unsteady structures for cavitation dynamics in a three-dimensional geometry of an axial flow water jet pump. With this study, it was desired to make sure that the cavitation cycles and periodical behaviours in [17] could be obtained with the interaction of the solver in OpenFOAM® and the models chosen, and it was successful. This study will provide an adequate numerical procedure for future cavitation studies related to marine engineering applications.

REFERENCES

[1] R. A. Furness and S. P. Hutton, "Experimental and Theoretical Studies of Two-Dimensional Fixed-Type Cavities," *J. Fluids Eng.*, pp. 515-521, 1975.

[2] P. A. Lush and P. I. Peters, "Visualisation of the cavitating flow in a venturi type duct using high-speed cine photography," *In Proceedings of the International Association of Hydraulic Engineering and Research Conference on Operating Problems of Pump Stations and Power Plants,* pp. 1-13, Amsterdam 1982.

[3] B. Stutz and J.-. L. Riboud, "Experiments on unsteady cavitation," *Exp. Fluids 21*, pp. 191-198, 1997.

[4] Y. Kawanami , H. Kato, H. Yamaguchi, M. Tanimura and Y. Tagaya, "Mechanism and Control of Cloud Cavitation," *Journal of Fluids Engineering*, vol. 119, no. 4, pp. 788-794, 1997.

[5] R. A. Arndt , C. S. Song, M. Kjeldsen and A. Keller, "Instability of Partial Cavitation: A Numerical/Experimental Approach," *In: Proceedings of 23rd Symposium on Naval Hydrodynamics, Office of Naval Research*, pp. 599-615, Val De Ruil France (National Academic Press, Washington, DC) 2000.

[6] K. R. Laberteaux and S. L. Ceccio, "Partial cavity flows. Part 1. Cavities forming on models without spanwise variation," *J. Fluid Mech.*, vol. vol, no. 431, pp. 1-41, 2001.

[7] J.-.. A. Astolfi, J.-.. B. Leroux, P. Dorange, J.-.. Y. Billard, F. Deniset and S. de La Fuente, "An Experimental Investigation of Cavitation Inception and Development on a Two-Dimensional Hydrofoil," *J. Ship Res.*, vol. 44, no. 04, pp. 259-269, 2000.

[8] J.-B. Leroux, J. A. Astolfi and J. Y. Billard, "An Experimental Study of Unsteady Partial Cavitation," *J. of Fluids Eng.*, vol. Vol., no. 126, pp. 94-101, 2004.

[9] B. Stutz and J.-.. L. Reboud, "Measurements within unsteady cavitation," *Experiments in Fluids*, vol. 29, no. 6, pp. 545-552, 2000.

[10] Q. Le, J.-P. Franc and J.-M. Michel , "Partial cavities : global behaviour and mean pressure distribution," *J. of Fluids Eng.*, pp. 243-248, 1993.

[11] P. A. Lush and S. R. Skipp, "High Speed Cine Observations of Cavitating Flow in a Duct," *Int. J. Heat and Fluid Flow*, vol. Vol., no. 7, pp. 283-290, 1986.

[12] S. Gopalan and J. Katz, "Flow structure and modeling issues in the closure region of attached cavitation," *Phys. Fluids*, vol. 12, no. 4, pp. 895-911, 2000.

[13] M. Callenaere, J.-P. Franc, J.-M. Michel and M. Riondet, "The cavitation instability induced by the development of a re-entrant jet," *J. Fluid Mech.*, pp. 223-256, 2001.

[14] D. De Lange, G. J. Bruin and L. Van Winjngaarden, "On the Mechanism of Cloud Cavitation-Experiment and Modelling," *In: Proceedings 2nd Int. Sypm. on Cavitation*, pp. 45-49, 1994.

[15] P. A. Lush and P. I. Peters, "Visualisation of the cavitating flow in a venturi type duct using high-speed cine photography," *In: Proceedings of the International Association of Hydraulic Engineering and Research Conference on Operating Problems of Pump Stations and Power Plant,* pp. 1-13, Amsterdam 1982.

[16] C. Song and Q. Qin, "Numerical Simulation of Unsteady Cavitating Flows," *In: Proceedings of the Fourth International Symposium on Cavitation*, 20-23 June 2001.

[17] J.-B. Leroux, O. Coutier-Delgosha and J.-A. Astolfi, "A joint experimental and numerical study of mechanisms associated to instability of partial cavitation on two-dimensional hydrofoil," *Phys. Fluids*, vol. 17, no. 5, pp. 1-20, 2005.

[18] A. Kubota, H. Kato and H. Yamaguchi, "A new modelling of cavitating flows: a numerical study of unsteady cavitation on a hydrofoil section," *J . Fluid Mech.*, vol. Vol., no. 240, pp. 59-96, 1992.

[19] O. Coutier-Delgosha, R. Fortes-Patella and J.

Reboud, "Evaluation of the Turbulence Model Influence on the Numerical Simulations of Unsteady Cavitation," *J. of Fluids Eng.*, vol. Vol., no. 125, pp. 38-45, 2003.

[20] E. Goncalves and R. F. Patella, "Numerical Simulation of Cavitating Flows with Homogeneous Models," *Computers and Fluids*, vol. 38, no. 2009, pp. 1-58, 2009.

[21] C. L. Merkle, J. Z. Feng and P. Bueow , "Computational modeling of the dynamics of sheet cavitation," *In: Proceedings of the 3rd International Symposium on Cavitation*, pp. 307-311, 1998.

[22] F. R. Kunz, A. D. Boger, R. D. Stinebring, T. S. Chyczewski, J. W. Lindau, H. J. Gibeling, S. Venkateswaran and T. R. Govindan, "A preconditioned Navier-Stokes method for two-phase flows with application to cavitation prediction," *Computers & Fluids*, vol. Vol., no. 29, pp. 849-875, 2000.

[23] G. H. Schnerr and J. Sauer, "Physical and Numerical Modeling of Unsteady Cavitation Dynamics," *In: ICMF-2001, 4th International Conference on Multiphase Flow*, May 27 - June 1 New Orleans, USA, 2001.

[24] A. Singhal, B. Yu, M. Athavale , H. Li and Y. Jiang, "Mathematical Basis and Validation of the Full Cavitation Model," *J. of Fluids Eng.*, vol. 124, no. 3, pp. 617-624, 2002.

[25] W. Yuann and G. H. Schnerr, "Optimization of Two-Phase Flow in Injection Nozzles–Interaction of Cavitation and External Jet Formation," *In:Proc.ASME Fluids Engineering Division,Summer Meeting*, 14-18 July, Montreal 2002.

[26] B. Pouffrey, R. Fortes-Patella and J. Reboud, "Numerical Simulation of Cavitating Flow around a 2D Hydrofoil : "A Barotropic Approach," *In: Fifth International Symposium on Cavitation (CAV2003)*, 1-4 November,Osaka 2003.

[27] T. S. Johansen, J. Wu and W. Shyy, "Filter-Based Unsteady RANS Computations," Unpublished, Technical Report, University of Florida, 2003.

[28] J. Wu, Y. Utturkar and W. Shyy , "Assesment of Modelling Strategies for Cavitating Flow Around a Hydrofoil," *In: Fifth International Symposium on Cavitation (CAV2003)*, 1-4 November,Osaka, Japan 2003.

[29] F. R. Menter, "Two-Equation Eddy-Viscosity Turbulence Models for Engineering Applications," *AIA A Journal*, vol. 32, no. 8, pp. 1598-1605, 1994.

[30] G. Zhang , W. Shi, D. Zhang , C. Wang and L. Zhou, "A Hybrid RANS/LES model for simulating time dependent cloud cavitating flow around a NACA66 hydrofoil," *Science China Technological Sciences*, vol. 59, no. 8, pp. 1252-1264, 2016.

[31] D.-S. Zhang, W. D. Shi, G. Zhang, J. Chen and B. M. van Esch, "Numerical analysis of cavitation shedding flow around a three-dimensional hydrofoil using an improved filter-based model'," *Journal of Hydrodynamics*, vol. 29, no. 2, pp. 361-375, 2017.

[32] B. Ji, X.-W. Luo, X.-X. Peng, Y. Zhang, Y.-L. Wu and H.-Y. Xu, "Numerical investigation of the Ventilated Cavitating Flow Around and Under-Water Vehicle Based on a Three-Component Cavitation Model," *Journal of Hydrodynamics*, vol. 22, no. 6, pp. 753-759, 2010.

[33] E. Alpman and E. L. Kavurmacıoğlu, "Investigation of Cavitation Noise of Marine Propeller using Computational Fluid Dynamics," *In: Ulusal Tesisat Mühendisliği Kongresi,* pp. 930-937, April 2019.

[34] B. Stutz and J.-L. Riboud, "Two phase flow structure of sheet cavitation," *Physics of Fluids*, vol. 9, no. 12, pp. 3678-3686, 1997.

[35] O. Coutier-Delgosha, J.-L. Reboud, B. Pouffary and R. Patella-Fortes, "Numerical Simulations of Unsteady Cavitating Flows : Some Applications and Open Problems," *In: Fifth International Symposium on Cavitation (CAV2003)*, 1-4 November, Osaka,Japan 2003.